PALEOCEANOGRAPHY, VOL. 24, PA4201, doi:10.1029/2008PA001674, 2009

Seasonal cycle as template for climate variability on astronomical timescales

Thomas Laepple[1] and Gerrit Lohmann[1]

Received 11 August 2008; revised 22 June 2009; accepted 2 July 2009; published 13 October 2009.

[1] We propose a new concept for insolation-driven temperature variability on orbital timescales. It relies on the modern relationship between insolation and temperature throughout the year. The method consists of (1) estimating empirical transfer functions between daily insolation and daily temperature and (2) applying these transfer functions on the long-term insolation to model the late Quaternary temperature evolution. On the basis of the observed insolation-temperature relationship, different temperature response regimes across the Earth are identified. Linear relationships dominate extratropical land areas whereas in midlatitude oceans, the seasonally varying mixed layer depth renders the temperature more sensitive to summer than to winter insolation. The temperature in monsoon regions and regions of seasonal sea ice cover also shows a seasonally varying response to insolation. These transfer functions characterize the shape of the seasonal cycle in temperature and influence the temperature evolution on orbital timescales by rectifying the insolation signal. On the basis of our seasonal template model, we estimate the temperature evolution of the last 750,000 years. The model largely reproduces the Holocene temperature trends as simulated by a coupled climate model. In the frequency domain, significant temperature variability in the eccentricity and semiprecession frequency band in the tropics is found. Midlatitudes are dominated by precession, and high latitudes are dominated by obliquity. Further, it is found that the expected frequency response highly depends on the location. Our local time-independent approach complements the global Milankovitch hypothesis (climate variations are driven by northern summer insolation) in explaining observed climate variability and potentially offers new insights in interpreting paleoclimate records.

Citation: Laepple, T., and G. Lohmann (2009), Seasonal cycle as template for climate variability on astronomical timescales, *Paleoceanography*, *24*, PA4201, doi:10.1029/2008PA001674.

1. Introduction

[2] The incoming solar radiation at the top of the atmosphere varies during the seasonal cycle as well as on multimillennial timescales. The long-term variations are caused by changes in the Earth's orbital geometry that affect the seasonal and latitudinal distribution of insolation. By computational analysis of the planetary system, these variations can be calculated to a high accuracy for the last millions of years [*Berger and Loutre*, 1991; *Berger*, 1978; *Laskar et al.*, 2004].

[3] Apart from shaping the seasonal cycle, the changes in the seasonal and latitudinal distribution of solar radiation are a primary driver for climate variability on multimillennial timescales. This relationship has been hypothesized for a long time [*Adhémar*, 1842; *Croll*, 1875; *Milankovitch*, 1941], and coherent variability of climate records and orbital parameters was found when geologists started to date climatic proxy records of ocean sediments [e.g., *Broecker and van Donk*, 1970; *Hays et al.*, 1976]. Despite important advances in the research of the orbitally forced climate variability the question remains how the climate system reacts on insolation forcing.

[4] One classical concept for the response of the climate system on orbital forcing was proposed by SPECMAP [*Imbrie et al.*, 1992]. Investigating a wide range of sediment cores, the authors concluded that insolation changes at high northern latitudes initiate a sequence of climate responses starting in the north, propagating to the south, and later returning north to force the ice sheets. Recent studies based on proxy data and models challenge this "northern pacing" viewpoint and suggest that local insolation at different latitudes also plays an important role. One example is the sensitivity of the climate in the tropical Pacific Ocean to local insolation that may influence the global climate [e.g., *Cane*, 1998]; In addition, proxy records from ocean sediment cores, representing the sea surface temperature (SST) show a different pattern between low and high latitudes [*Pahnke and Sachs*, 2006]; Modeling work shows that temperature variability in Antarctica may be driven by local insolation [*Huybers and Denton*, 2008]; Studies from coupled atmosphere-ocean general circulation models (AOGCM) suggest that the strength of the monsoons is influenced by local insolation [e.g., *Clemens et al.*, 1991]; A recent study compared transient AOGCM simulations of the Holocene with temperature proxy data [*Lorenz et al.*, 2006] and emphasized the heterogeneous pattern of the temperature response to insolation forcing.

[1]Alfred Wegener Institute for Polar and Marine Research, Bremerhaven, Germany.

0883-8305/09/2008PA001674$12.00

[5] The climate response to insolation is nonlinear: Variations, coherent to the precession of the perihelion are found in a large number of temperature proxies [e.g., *Imbrie et al.*, 1992; *Pahnke et al.*, 2003], but the precession of the perihelion does not affect the annual mean insolation at any point on Earth [*Rubincam*, 1994]. One particular nonlinearity is proposed in the classical studies of *Milankovitch* [1941] and SPECMAP [*Imbrie et al.*, 1992] who state that the summer insolation intensity is the driving force linking the sensitivity of snow ablation to summer radiation. This concept was refined by the summer energy concept of *Huybers* [2006] and *Huybers and Tziperman* [2008] who point to the role of the integrated summer insolation as driver of snow ablation. Part of the glacial-interglacial variability can be understood by these concepts. However, it seems unlikely that summer is the dominating season on all orbital timescales and in all regions.

[6] Hence, nonlinear and spatially resolved models are needed for the understanding of the climate response on insolation forcing. For this purpose energy balance models were used and could show the important role of the land-sea distribution on the orbital temperature variability found in proxy records [*Short et al.*, 1991]. However, important feedback mechanisms were neglected by using a linear approach. On the other hand, three-dimensional climate models provide a physically consistent approach and show the importance of the local forcing, especially in the tropics [e.g., *Clement et al.*, 2004; *Tuenter et al.*, 2003]. However, climate model simulations are limited in length by computing resources. Further, a simulation from a complex model does not imply a direct understanding of the mechanisms involved [*Held*, 2005].

[7] Here we make use of the modern seasonal cycle of temperature to derive the insolation-temperature relationship on reanalysis data. We propose a simple concept: the local temperature response to insolation has the same transfer function on astronomical timescales and on seasonal time scales. Our method consists of (1) estimating empirical transfer functions between daily insolation and daily temperature and (2) applying these transfer functions on the long-term insolation history to model the past temperature evolution. Our technique includes nonlinearities that are shaping the modern seasonal cycle to derive a local model for the temperature response. Since the method does not include slow feedbacks such as the ablation of ice sheets, that is a multiyear process, or feedbacks caused by the interaction of the carbon cycle and the climate system, it cannot be used to estimate glacial-interglacial climate variability. However, the empirical approach includes all "fast" feedback (seasonal time scale) processes and allows a systematic estimation of their influence on the regional temperature evolution of the Quaternary.

2. Data and Methods

2.1. Temperature Data and Holocene Model Simulation

[8] To derive the present-day temperature cycle, we use daily near-surface temperature data from the National Centers for Environmental Prediction (NCEP) reanalysis [*Kalnay et al.*, 1996]. The data are available on a $2.5 \times 2.5°$ horizontal grid, and we examine the mean seasonal cycle derived from the years 1948–2007 after removing the leap days. For the comparison of our technique with complex climate models, we use a transient simulation from the atmosphere-ocean general circulation model ECHO–G [*Lorenz et al.*, 2006; *Lorenz and Lohmann*, 2004]. This simulation covers the last 7000 years from the mid-Holocene until today, changing only the orbital forcing. It consists of a two member simulation, performed with a 10 times accelerated insolation forcing (700 model years). In our study, we analyze the near-surface temperature and the sea ice coverage averaged over the two ensemble members.

2.2. Parameterizing the Temperature Response to Insolation

[9] The annual cycle of surface temperature can be approximated as a linear function of insolation after including a time lag to represent the thermal inertia [e.g., *Huybers*, 2006]:

$$T_{surf}(t,x) = a(x) + b(x) * I(t - \tau(x), x) \qquad (1)$$

Here T_{surf} is the surface temperature, I the insolation, t the time of the year, x the location, a is a free parameter, b represents the linear temperature sensitivity and τ the time lag between insolation and temperature.

[10] Because in some regions the local temperature is more sensitive to summer or winter insolation we introduce a nonlinear extension of this model by applying a polynomial transfer function between temperature and insolation. The temperature is now modeled as

$$\begin{aligned} T_{surf}(t,x) &= F(I(t-\tau(x),x)) \text{ with} \\ F(I,x) &= a(x) + b(x)I + c(x)I^2 + d(x)I^3 \end{aligned} \qquad (2)$$

The coefficients a .. d as well as τ are determined by a least squares fit on the daily data. In preliminary studies, we found a third-order polynomial to be a tradeoff between explained variance and model complexity. The results are not sensitive to this choice, as similar results are obtained using a second- or fourth-order polynomial.

[11] We estimate the linear and polynomial transfer functions between local insolation and local surface temperature on a 5×5 degree horizontal grid, using daily reanalysis data. The approach is demonstrated for one grid point in the North Pacific (40°N 200°E) (Figure 1). At this location, the temperature lags insolation by approximately two months, and the summer temperature highs and winter temperature lows are narrower and broader, respectively, than those in insolation. Therefore, only a polynomial model can accurately represent the temperature cycle as function of the insolation cycle. The transfer function shows a nonlinear behavior with smaller temperature sensitivity in winter than in summer.

2.3. Insolation Forcing

[12] The orbital forcing is controlled by three main parameters: the departure of the elliptical orbit with the

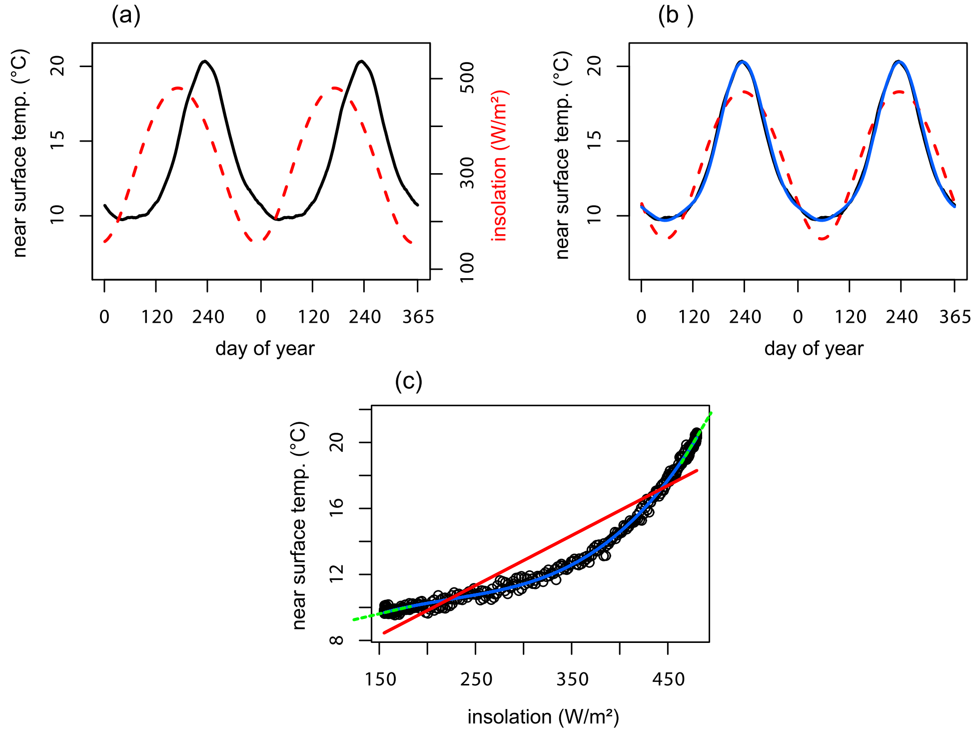

Figure 1. Relationship of the seasonal cycle of insolation and near-surface temperature in the North Pacific (200°E, 40°N). (a) Mean seasonal temperature cycle, smoothed by a 20-day filter (black) and mean daily insolation (red dashed). (b) Mean seasonal temperature cycle (black) and the seasonal cycle as predicted by a linear model (red dashed) and a polynomial model (blue). As the polynomial model explains most of the seasonal cycle, the black line is hidden by the blue line. (c) The best fitting linear model (red) and polynomial model (blue) are shown along with the temperature (black circles). Additionally, the summer and winter sensitivities are shown (green dotted lines).

Sun in one of the two foci from circularity (eccentricity), the time of the Earth's passage through its perihelion (precession), and the tilt of its rotation axis (obliquity) [e.g., *Milankovitch*, 1941]. Changes in these parameters cause changes in the seasonal and spatial distribution of insolation. The precession which has primary periodicities near 19 and 23 thousand years (ka) determines the strength of the seasonal cycle with a strong (weak) seasonality if the local summer coincides with perihelion (aphelion). The forcing is therefore antisymmetric between the hemispheres. The insolation is only redistributed between summer and winter, and the annual net effect is zero [e.g., *Loutre et al.*, 2004]. The eccentricity varies primarily at periodicities near 100 and 400 ka and modulates the seasonal difference in Earth-Sun distance and therefore the strength of the precession. It has only a small effect on the annual mean insolation (<0.5%). Obliquity which has primary periodicities near 41 ka with some energy in the 54 and 29 ka bands affects the seasonal contrast and the latitudinal gradient of insolation. High obliquity results in more high-latitude summer insolation at the expense of low-latitude summer insolation. Obliquity explains most of the variance in the annual insolation [e.g., *Loutre et al.*, 2004], and the effect is symmetric between the hemispheres but antisymmetric between the tropics and high latitudes. For a more rigorous description of the seasonal and annual insolation forcing see *Loutre et al.* [2004].

[13] In our study, we use the daily insolation forcing for the last 750 ka, calculated on the basis of the work by *Berger* [1978]. Whereas newer calculation schemes exist, which are accurate beyond millions of years [*Laskar et al.*, 2004], the differences between the calculation schemes are small for the time span covered in our study. We would like to note that in this study we refer to summer as the local summer defined by the local insolation maximum, not by a fixed date in the year.

2.4. Application on the Long-Term Climate

[14] The present-day transfer functions are applied to the daily insolation over the last 750 ka. The resulting temperature time series are analyzed in the spectral domain. Both steps are performed on an equidistant 5 $\times$ 5 degree horizontal grid. Prior to the spectral analysis, the time series are averaged to 100-year mean values to reduce computing time. This approach was compared to the direct application of the spectral analysis on the daily data and was found to be accurate enough for the purpose of this study.

3. Results

3.1. Present-Day Transfer Function

[15] A simple polynomial transfer function of insolation (equation (2)) accounts for between 30 and 99% of the variance in observed temperature (Figure 2a). This

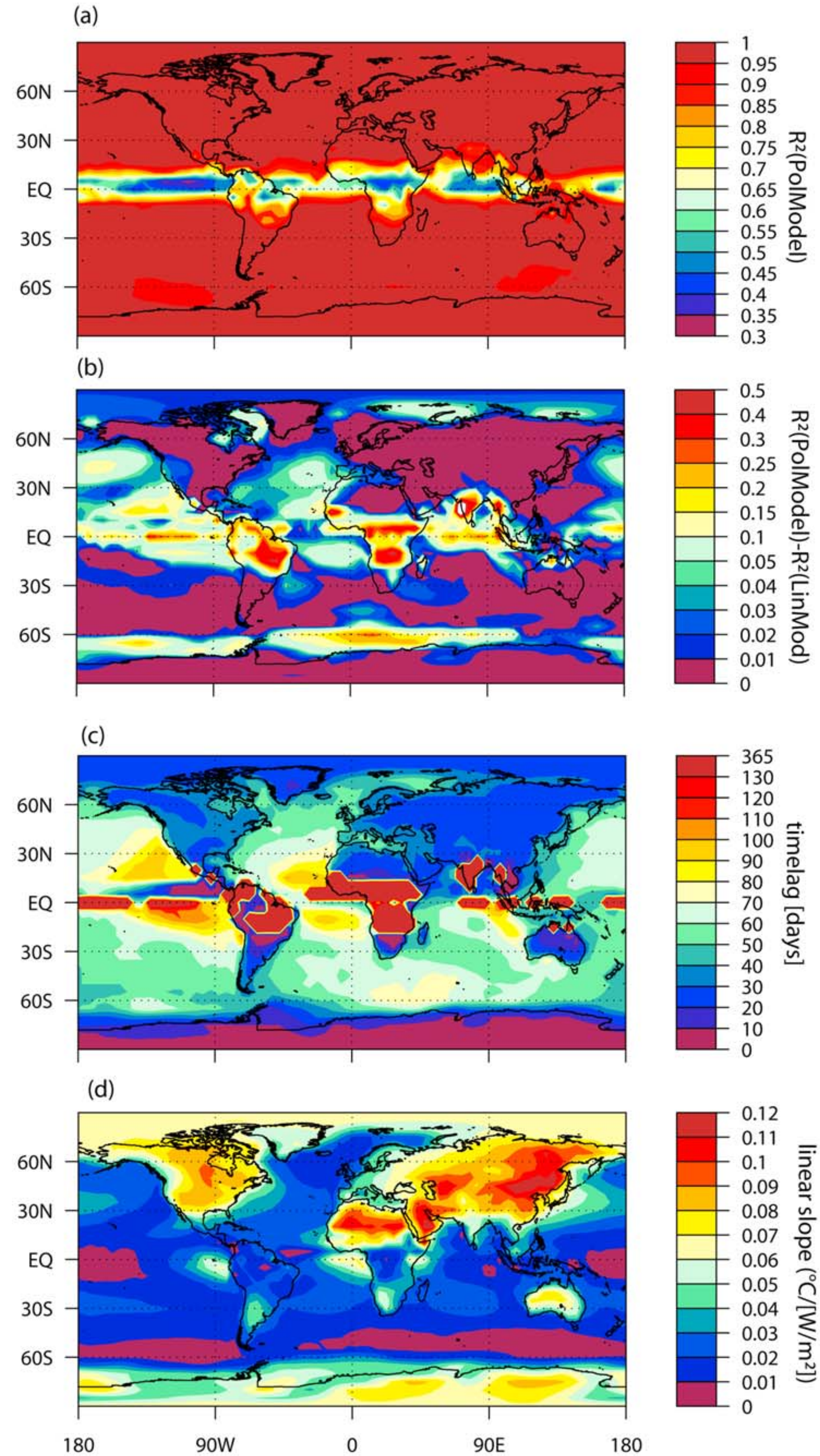
(a)
60N
30N
EQ
30S
60S
1
0.95
0.9
0.85
0.8
0.75
0.7
0.65
0.6
0.55
0.5
0.45
0.4
0.35
0.3
R²(PolModel)
(b)
0.5
0.4
0.3
0.25
0.2
0.15
0.1
0.05
0.04
0.03
0.02
0.01
0
R²(PolModel)-R²(LinMod)
(c)
365
130
120
110
100
90
80
70
60
50
40
30
20
10
0
timelag [days]
(d)
0.12
0.11
0.1
0.09
0.08
0.07
0.06
0.05
0.04
0.03
0.02
0.01
0
linear slope (°C/[W/m²])
180
90W
0
90E
180

Figure 2

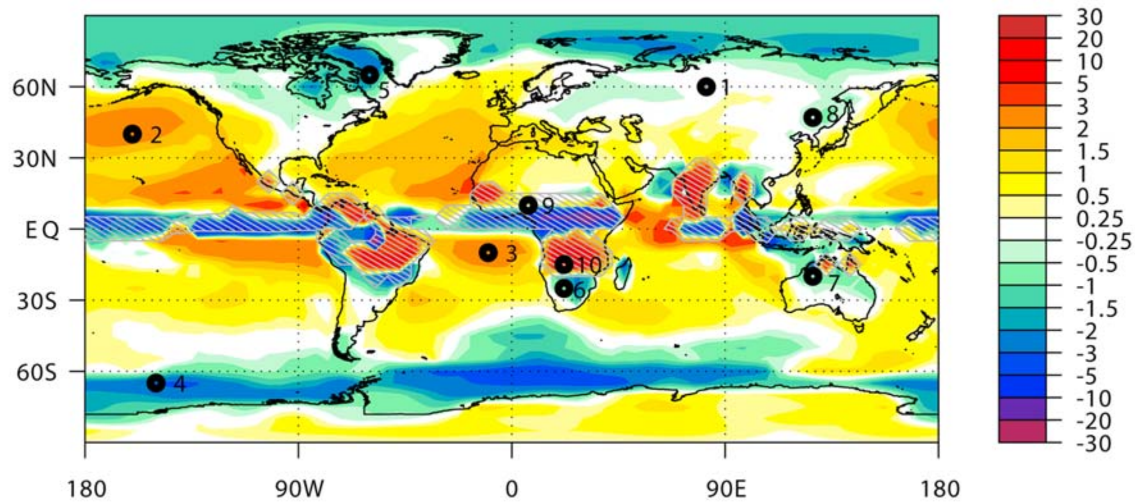

Figure 3. Global distribution of seasonal sensitivity. This is defined as normalized difference of the temperature sensitivity at maximum and minimum insolation. Positive (negative) values correspond to summer (winter) sensitive regions. Regions with $R^2 < 50\%$ or $\tau > 130$ days are hatched. Black circles and numbers mark the points for which Figure 4 shows the transfer functions.

explained variance (R^2) depends strongly on latitude. In most extratropical regions the R^2 of the polynomial model is higher than 0.95 with some exceptions around the Antarctic continent where it decreases to 0.9–0.95. In the tropics, the explained variance is reduced toward the equator, and some areas with R^2 of 0.3 are detected. To remind the reader to be careful with the interpretation of these regions, we shade the areas with $R^2 < 0.5$ in the remaining part of this study.

[16] The differences in R^2 between the polynomial model and the linear model show the regions in which the nonlinear term adds skill to the model (Figure 2b). This is the case in seasonal sea ice areas, in the central North Pacific and North Atlantic, in the tropical oceans, and in the monsoon areas. At the equator, the higher R^2 of the polynomial model relative to the linear model has to be interpreted with care as the R^2 in this region is small.

[17] The time lag τ between insolation forcing and temperature response varies across different regions (Figure 2c). Over land, τ is small, mostly less than one month, with a minimum over the Antarctic continent, where the temperature almost immediately follows the insolation. Over the oceans, τ varies between one and three months with maxima in the subtropics. In the monsoon areas of India, Central America, West Africa, and Central Africa, we detect τ to be of more than four months. These high values suggest that the local model has no direct physical meaning in these regions and can also be interpreted as negative time lag (temperature leads insolation). We therefore mark these regions with $\tau > 130$ days in the remainder of this study. Reasons for the high τ values over the tropical land areas are the influence of remote temperatures that affect the local annual cycle of temperature by changes in cloudiness and evaporation [*Biasutti et al.*, 2003]. Additionally the strong internal stochastic internal variability and the small amplitude of the tropical seasonal cycle lead to high estimation errors in the parameters.

[18] The linear sensitivity of temperature on insolation (Figure 2d) displays a clear distinction between continental areas with high sensitivity and open ocean areas with low sensitivity to insolation. On the continents, the temperature sensitivity exhibits an east-west gradient. In areas downwind of the continents, regions of higher temperature sensitivities are detected.

[19] To describe the shape of the fitted polynomial transfer function, we introduce the diagnostic seasonal sensitivity (S) that is zero for a linear insolation-temperature relationship, positive when the temperature is summer sensitive (one unit insolation change affects the temperature more in summer than in winter), and negative when the temperature is winter sensitive (insolation changes affect the temperature more in winter than in summer). It is defined as the difference of the derivatives of the polynomial transfer function F (from equation (2)) at maximum local insolation $I_{\max}$ and minimum local insolation $I_{\min}$ (see green lines in Figure 1c), normalized by the linear sensitivity b (from equation (1)):

$$S(x) = \frac{\frac{\partial F}{\partial I}(I_{\max}, x) - \frac{\partial F}{\partial I}(I_{\min}, x)}{b(x)} \tag{3}$$

[20] The seasonal sensitivity map (Figure 3) shows positive values over most oceanic regions with the strongest summer sensitivity observed in the North Pacific and in the

Figure 2. Model diagnostics of the transfer model fit. (a) Explained variance in temperature (R^2) of the polynomial model. (b) Difference in R^2 between the polynomial and linear models. (c) Time lag parameter τ. Please note that all time lags > 130 days are plotted in one color. (d) Slope parameter of the linear model.

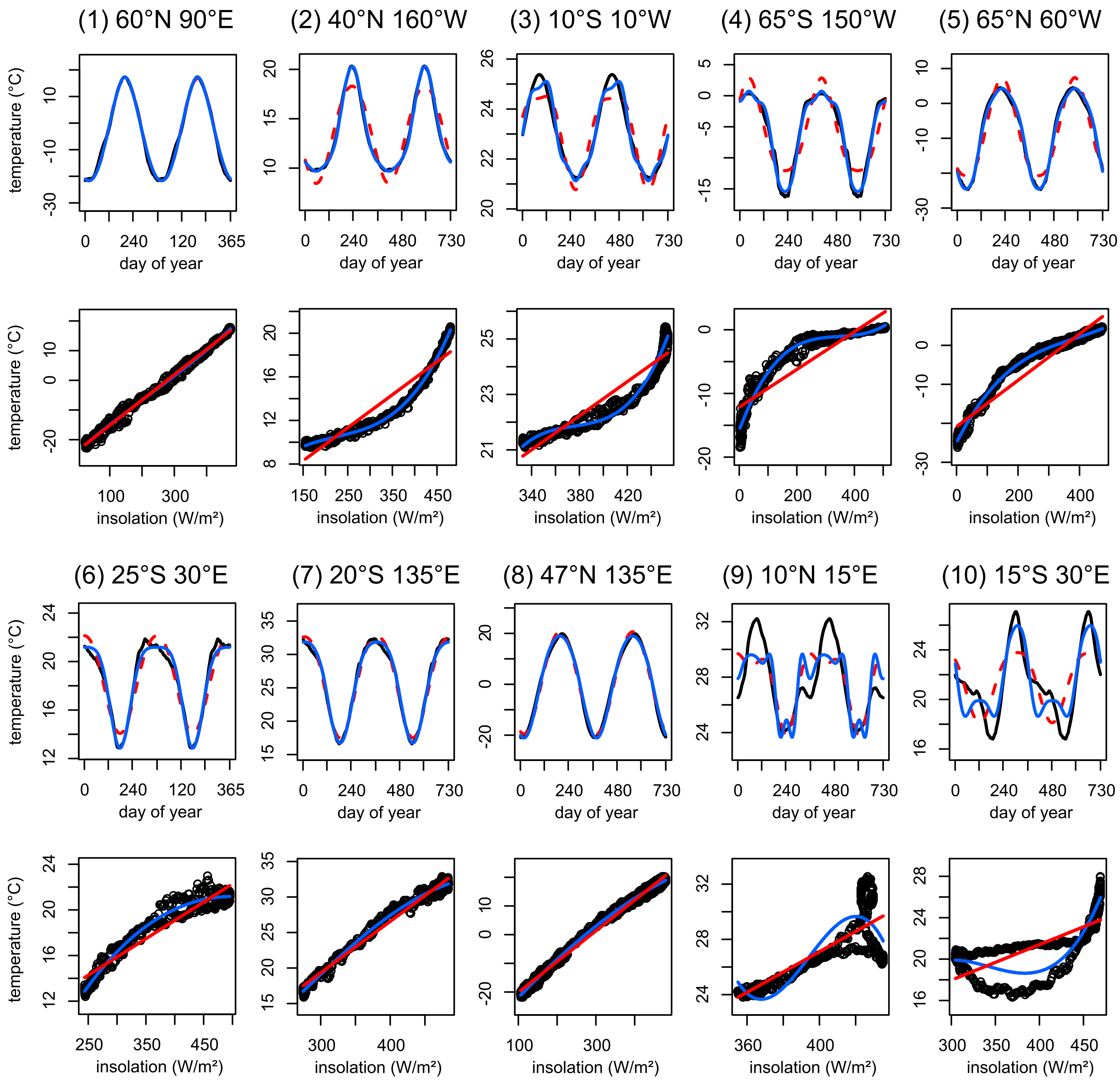

Figure 4. Seasonal cycles and transfer functions for selected points which are marked in Figure 3. Mean seasonal temperature cycle (black), the seasonal cycle as predicted by a linear model (red dashed) and a polynomial model (blue). The linear model (red) and polynomial model (blue) are shown along with the temperature (black circles).

subtropical oceans. In polar latitudes, the Arctic and the Antarctic sea ice regions are winter sensitive. The temperature over the midlatitude continents behaves linearly. In the tropics, the structure is more complicated as strongly summer sensitive as well as winter sensitive regions are detected. However, these regions also have a low R^2 and/or a negative time lag.

[21] We propose a qualitative classification of the regionally different response functions to several response regimes. These are based upon the shape of the transfer function and are exemplified by specific locations (Figure 4).

[22] 1. Over extratropical continental areas, the response function is close to linear [*Huybers*, 2006]. One example is Central Asia (Figure 4, transfer function 1).

[23] 2. Enhanced mixing of the ocean surface layer in local winter and related changes in seasonal mixed layer depth (MLD), defined as depth with nearly uniform temperature, lead to a stronger damping of the winter temperature response in the midlatitude and subtropical oceans. A qualitative attribution of the summer sensitivity to MLD changes can be made by comparing the patterns to a seasonal MLD climatology [*Kara et al.*, 2003]. Examples for this regime are areas in the North Pacific

(Figure 4, transfer function 2) and southern tropical Atlantic (Figure 4, transfer function 3). In the seasonal cycles, the summer sensitivity is detected as narrow summers and broad winters.

[24] 3. Regions with seasonal sea ice cover [*Rayner et al.*, 2003] are more sensitive to winter insolation. In winter, the sea ice cover insulates the warmer ocean from the atmosphere, providing an additional cooling [e.g., *Jackson and Broccoli*, 2003]. This applies around Antarctica (Figure 4, transfer function 4) as well as at the arctic sea ice boundary (Figure 4, transfer function 5). In the response function, this is detected as a division into a summer part with a small insolation-temperature slope and a winter part with a large slope.

[25] 4. Our transfer function shows a winter sensitivity in regions which are classical monsoon areas [e.g., *Lau et al.*, 2007]. These regional climates are characterized by a summer precipitation maximum driven by seasonal winds. The summer precipitation leads to evaporative cooling of the surface temperature and acts as a negative feedback when we regard the temperature as function of local insolation. Examples are South Africa (Figure 4, transfer function 6), North Australia (Figure 4, transfer function 7) and East Asia (Figure 4, transfer function 8). The seasonal cycles are characterized by broad summers, which are represented by a small summer slope in the transfer functions.

[26] 5. In some regions in the tropics, including the Asian and African monsoon, the local polynomial model cannot well explain the seasonal cycle [*Biasutti et al.*, 2003]. Examples are shown for West Africa (Figure 4, transfer function 9) and Central Africa (Figure 4, transfer function 10). We still apply our polynomial model which leads to a strongly nonlinear response. A similar nonlocality can be found in ocean regions around the equator. In these regions, nonlocal effects like coastal upwelling modulated by alongshore winds and changes in heat loss due to annual variations in wind speed have a strong effect [*Carton and Zhou*, 1997].

3.2. Application to the Mid-Holocene

[27] As a test of our concept, we predict the surface temperature trends between the mid-Holocene (7 ka) and preindustrial (PI) conditions by applying the linear and polynomial transfer functions on the historical insolation over the last 7 ka. The results are compared to transient simulations of the coupled AOGCM ECHO-G [*Lorenz and Lohmann*, 2004].

[28] The surface temperature trend in annual mean temperatures, predicted assuming a linear response to insolation forcing, shows a weak tripole pattern (Figure 5a). A cooling trend from the mid-Holocene to PI in the polar latitudes north of 60°N and south of 60°S of up to 0.5°C/7 ka and a slight warming trend of less than 0.1°C/7 ka in tropical land areas are found. Using the polynomial transfer function, the temperature trend pattern is more complex and the trends are stronger (Figure 5b). The large-scale patterns are a cooling trend at high latitudes and a dipole pattern in the tropics/midlatitudes, consisting of a cooling trend in the Northern Hemisphere and a warming trend in the Southern Hemisphere.

[29] The temperature trend pattern as simulated by the ECHO-G climate model (Figure 5c) has a strong similarity with the patterns of the polynomial template model. Again a cooling trend in the high latitudes and a dipole pattern in the midlatitudes (cooling in the Northern Hemisphere, warming in the Southern Hemisphere) are found. Regional warming in the Sahel, South Asia, and the east coast of China and a cooling trend in North Australia, South Africa, and Madagascar are detected, in line with the polynomial model.

[30] Remarkably, signatures of all the response regimes that we discussed for the present-day temperature cycle are detected in the Holocene temperature trends in the data-based polynomial model as well as in the ECHO-G simulation. Regions in the Northern Hemisphere that show summer sensitivity in the present-day seasonal cycle show a cooling trend and winter sensitive regions a warming trend. In the Southern Hemisphere, the relationship is inverted. In the polynomial model, temperatures in the seasonal mixing regime show a cooling trend of up to 1°C in the Northern Hemisphere, for example in the North Pacific. In the Southern Hemisphere, the corresponding warming trend is 0.2–0.5°C. Similar patterns are found in the GCM simulation, but details in the spatial extent and strength of the trend differ from the polynomial model.

[31] The predictions of the polynomial template model for regions with seasonal sea ice cover are too warm in the Northern Hemisphere and too cool in the Southern Hemisphere compared to the GCM results. Reasons for this mismatch in polar latitudes are changes in the mean sea ice cover in the GCM simulation (hatched areas in Figure 5c) that strongly affect the surface temperature. This leads to strong cooling trends in most sea ice areas in the GCM simulations except in some patches in the Southern Hemisphere at 100°W and 25°W that show a decrease in sea ice cover and therefore a warming trend in the GCM. A similar mechanism can explain the differences in the temperature trend between the ECHO-G simulations and the template model over Europe and central North America. The present-day seasonal snow cover leads to a slight winter sensitivity (see Figure 3), and therefore a warming trend in the template model predictions. In ECHO-G, the mean snow cover shows a positive trend which leads to a cooling. Since the mid-Holocene, precipitation in the monsoon areas has decreased in the Northern Hemisphere and increased in the Southern Hemisphere [*Liu et al.*, 2004]. This lead to a warming trend in the Northern Hemisphere regions and a cooling trend in the Southern Hemisphere regions. These changes are reproduced by the ECHO-G model as well as with the polynomial model in all monsoon regions (South Africa, North Australia, East Asia, and West Africa) except the Indian monsoon region where the polynomial model predicts a trend in the wrong direction. A reduction in monsoon precipitation in Mexico [*Liu et al.*, 2004] leads to a warming trend in the GCM simulation which is not captured by the polynomial model. Moreover, changes in the atmospheric circulation as well as climate feedbacks simulated by the GCM are not included in our data-based approach. Such feedbacks are likely responsible for the

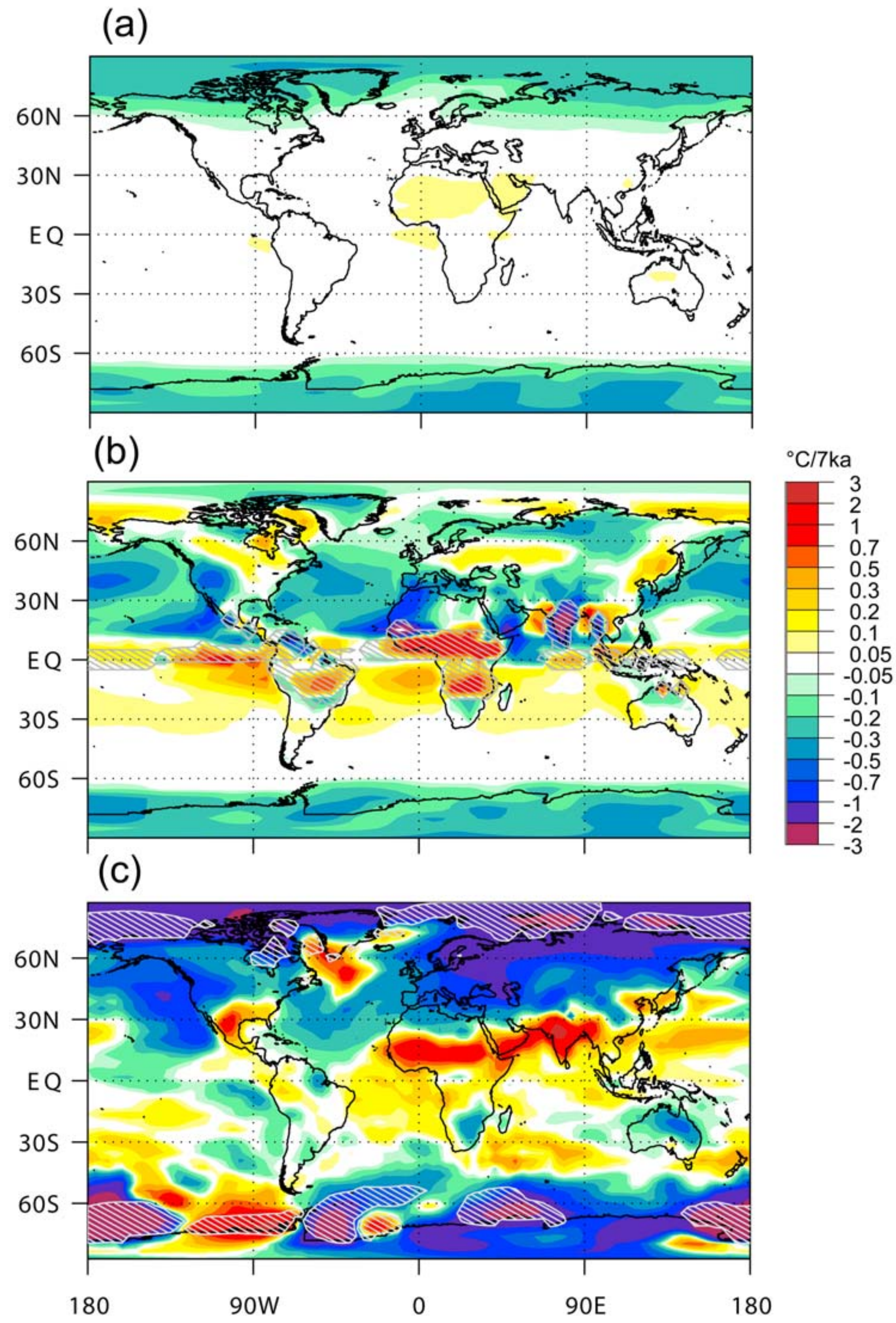

Figure 5. Temperature trend between the mid-Holocene (7 ka) and PI (0 ka) in °C/7 ka. (a) As predicted by the linear model, (b) as predicted by the polynomial model, and (c) from the ECHO-G AOGCM simulation [*Lorenz et al.*, 2006]. In Figure 5b regions with R^2 < 50% or τ > 130 days are hatched. In Figure 5c regions with a sea ice trend > 3%/ka corresponding to a 0.5–1°C/7 ka temperature trend, assuming a sea ice temperature of −15 to −30°C, are hatched.

mismatch between both approaches in the North Atlantic. In this region, the GCM simulates a change in the mean state of the North Atlantic oscillation (NAO) and associated high-latitude temperature and sea ice changes [*Lorenz and Lohmann*, 2004; *Lohmann et al.*, 2005].

3.3. Impact on Long-Term Variability

[32] As a further application of our linear and polynomial model, we examine the temperature evolution of the last 750 ka. The results are analyzed in the spectral domain by using the periodogram of the time series [*Bloomfield*, 1976].

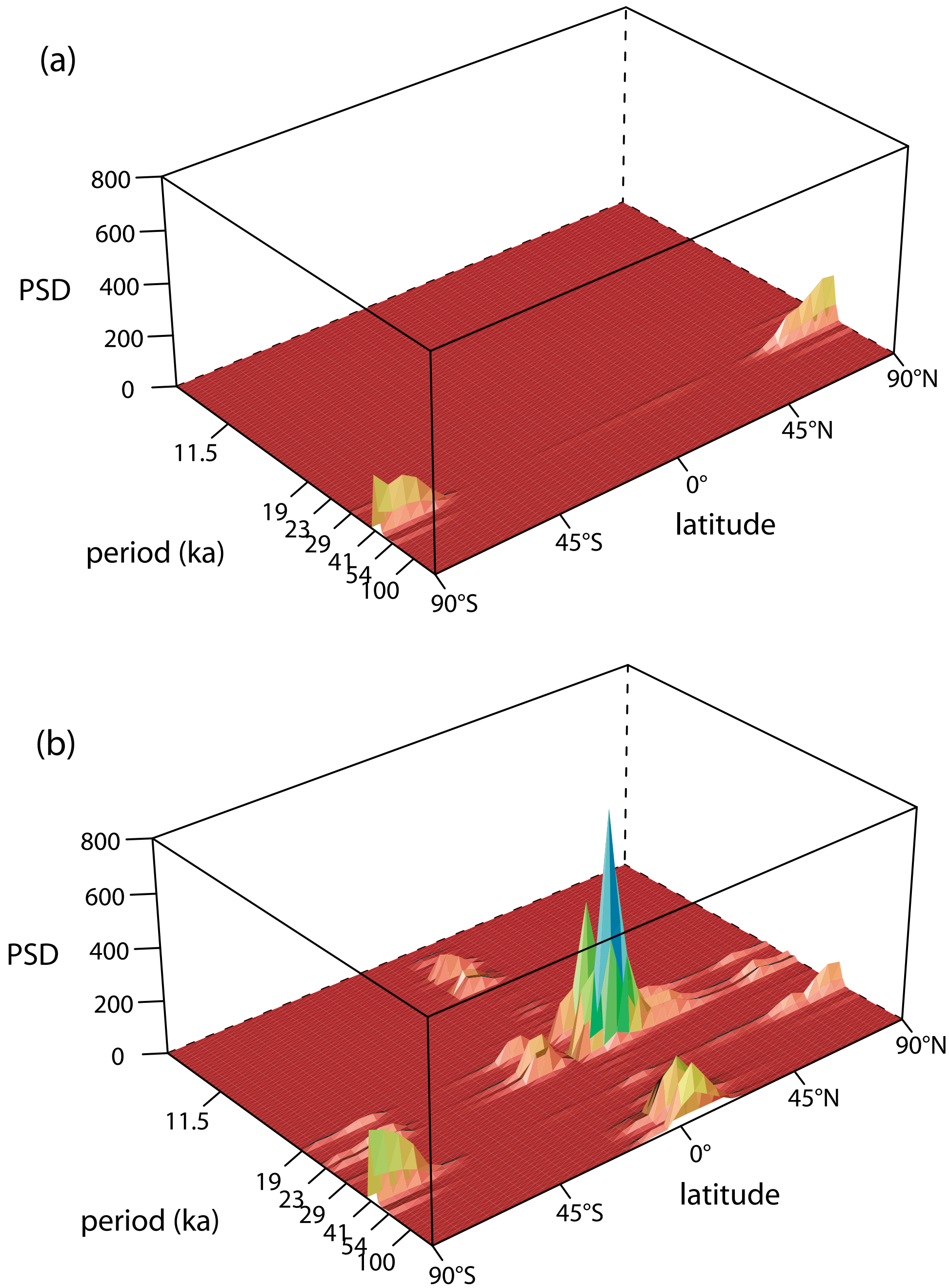

Figure 6. Zonal mean frequency spectra of the surface temperature of the last 750 ka as predicted by (a) the linear model and (b) the polynomial model.

[33] The zonal mean temperature spectra strongly depend on whether we use the linear or the polynomial transfer function (Figure 6). When the linear transfer function is used, only power in the obliquity band (41 ka, 29 ka and 54 ka) is detected (Figure 6a). Most of the obliquity band variability is found at high latitudes with a small secondary maximum in the tropics. Interestingly, the polynomial transfer function has a significant effect on the spectra (Figure 6b). Strong precession bands at 19 and 23 ka are detected with a maximum in the subtropics. Additionally, the obliquity bands spread more into the midlatitudes, especially in the Northern Hemisphere. Remarkably, significant spectral power is detected in the tropics in the eccentricity (100 ka, 400 ka) and semiprecession (9.5–11.5 ka) frequency bands. The results are not symmetric between the hemispheres, with higher precession amplitudes in the northern subtropics and a stronger obliquity signal in the southern polar regions. When we compare the orbital bands, the obliquity signal dominates the polar latitudes, and precession is the most important frequency on the remaining parts of the world.

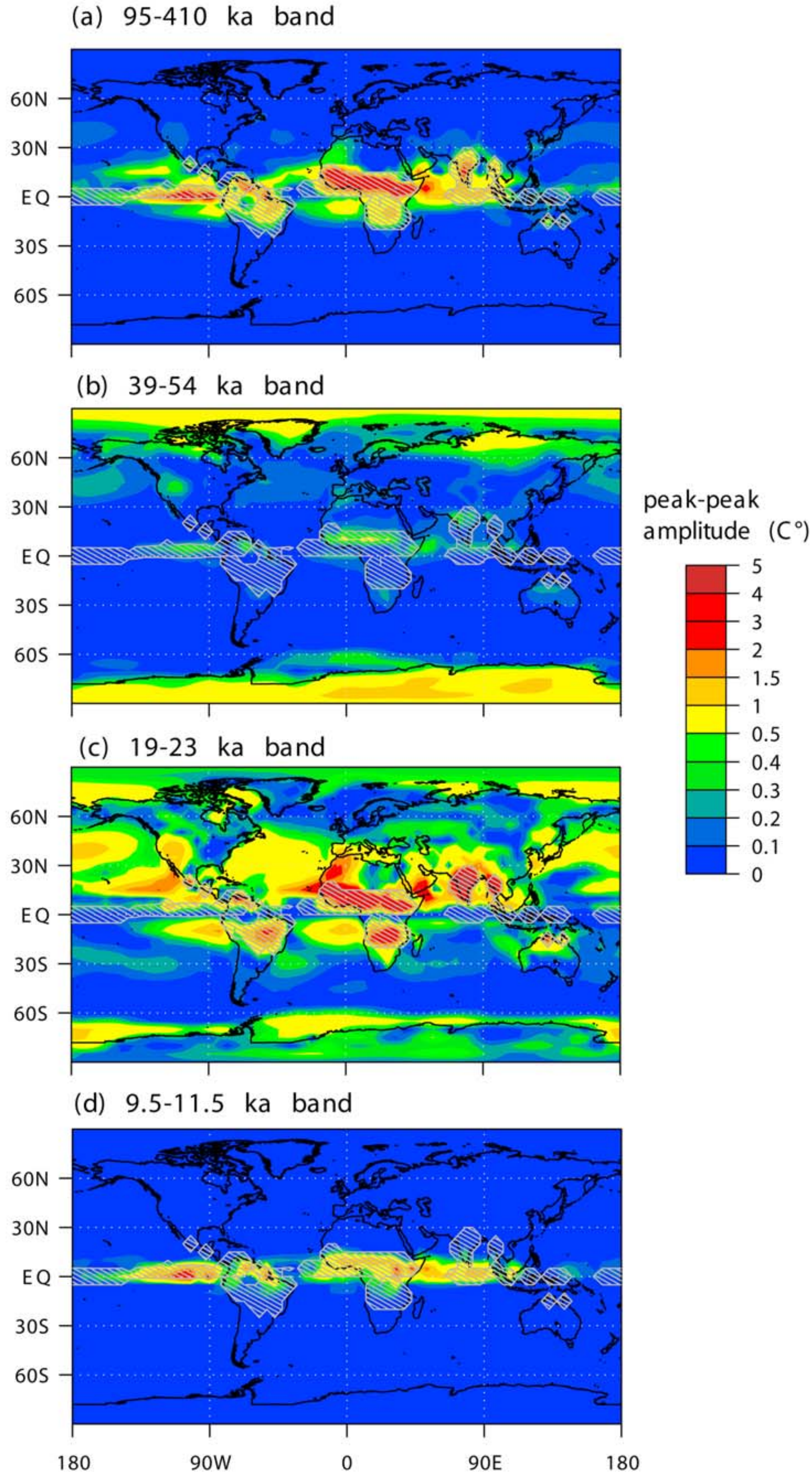
(a) 95-410 ka band
(b) 39-54 ka band
(c) 19-23 ka band
(d) 9.5-11.5 ka band
60N
30N
EQ
30S
60S
180
90W
0
90E
180
peak-peak amplitude (C°)
5
4
3
2
1.5
1
0.5
0.4
0.3
0.2
0.1
0

Figure 7

[34] As shown for the Holocene in section 3.2, the temperature response to insolation changes is also zonally dependent. We therefore analyze the spatially resolved maps of spectral amplitudes integrated over the orbital bands eccentricity (95–410 ka), obliquity (39–54 ka), precession (19–23 ka), and semiprecession (9.5–11.5 ka). This analysis is only performed with the polynomial model. To simplify the comparison with short proxy records, we choose temperature peak to peak (pp) units. These units correspond to the temperature difference between the two extremes of the orbital parameter and are related to the variance (var) as: $pp = \sqrt{2 * var} * 2$. Variability in the eccentricity band (Figure 7a) is mainly simulated in the tropics with amplitudes up to 5°C in West Africa and the East Pacific. An eccentricity signal is detected up to 45°N, mainly in the North Pacific and North Atlantic with amplitudes of 0.1–0.2°C. We note, however, that the highest amplitudes are found in the regions where the polynomial model does not perform well for the seasonal cycle. The obliquity signal (Figure 7b) is mainly present in high latitudes, and the highest amplitudes are found on the Antarctic continent (1–1.5°C) and in the northern polar regions (around 1°C). The polynomial template model also predicts an obliquity signal in monsoon regions and in the North Pacific and North Atlantic oceans. Globally, the dominating astronomical component is the precession (Figure 7c) with highest amplitudes in the tropical regions, namely West Africa, India and Central Africa of up to 5°C. Again, the highest amplitudes are found in the areas where the polynomial model does not fit well for the present-day seasonal cycle. Over the midlatitude oceans, amplitudes of 0.5–1.5°C are found, that are generally higher in the Northern Hemisphere. Another band of precession is found in the polar seasonal sea ice covered regions.

4. Discussion

[35] In our seasonal template model, the nonlinearities, shaping the seasonal cycle have a strong impact on the temperature response on insolation changes. In section 4.1 we will discuss how the insolation forcing interacts with the transfer function to produce the temperature variability patterns.

4.1. Holocene Temperature Response to Insolation

[36] Between the mid-Holocene (7 ka) and today (0 ka), the tilt of the Earth's axis decreased from 24.2 to 23.4 degrees. Further, the perihelion shifted from September to January. The temperature responses (Figures 5a and 5b) can be explained as interplay of the following effects.

[37] 1. The larger tilt in the mid-Holocene increases the summer and annual mean insolation in high latitudes and leads to a small reduction in annual mean insolation in the tropics. This leads to a tripole pattern in the temperature trends (Figure 5a) simulated by the linear model with cooling in the polar regions and slight warming in the tropics. The same effect also applies when the polynomial temperature response is used (Figure 5b), but as we will discuss now, when the nonlinear model is used, the effects of the change in the date of perihelion are dominating the response in the extratropical regions.

[38] 2. The changes in the date of perihelion influence the strength of the seasonal cycle. In the Northern Hemisphere, the insolation intensity is increased in mid-Holocene summer, but decreased in mid-Holocene winter. This has no influence on the integrated annual insolation [*Rubincam*, 1994] and therefore no effect on the linear response pattern (Figure 5a). However, under a nonlinear response summer and winter anomalies do not balance each other anymore. Therefore, summer sensitive regions lead to warmer surface temperatures and winter sensitive regions lead to colder temperatures in the mid-Holocene. In the Southern Hemisphere, the response is antisymmetric.

[39] 3. The temperature response is scaled by the local temperature sensitivity (Figure 2d). This local sensitivity is higher over land because of the smaller heat capacity. Therefore, the response to changes in the obliquity parameter is mainly limited to continents.

[40] A comparison with the results from the AOGCM ECHO-G (Figure 5c) shows that the nonlinear template model is much closer to the GCM results than the linear model. All the nonlinearities we identified in the seasonal cycle have an imprint on the long-term temperature trend which is also found in the GCM results. Even in the regions in which the local model does not work well for the present-day seasonal cycle, the predicted patterns are comparable to the GCM results. This suggests that a large part of nonlinearity in the climate system can be explored by the system's response to the seasonal cycle of insolation. In some regions, the polynomial template model underestimates the amplitudes and does not represent the high-latitude trends well. This is caused by climate feedbacks, such as long-term changes in sea ice cover, snow cover and ocean and vegetation feedbacks, which are slower than the annual time scale and are therefore not represented in the seasonal cycle [*Ganopolski et al.*, 1998; *Wohlfahrt et al.*, 2004]. We therefore propose the template model as lower estimate of the climate variability driven by local insolation.

4.2. Long-Term Temperature Response to Insolation

[41] The mechanisms of the division of the orbital forcing into its different components by the nonlinearity of the temperature response are similar to those just described for the Holocene case. The variability in the obliquity parameter primarily affects the high latitudes. As it also affects the annual mean insolation it has an imprint on the temperature modeled by the linear (Figure 6a) as well as by the polynomial model (Figures 6b and 7b). The precession of the equinoxes only affects the nonlinear response (Figures 6b and 7c) as insolation maxima related to the precession signal in one season are balanced by opposing

Figure 7. Global maps of the amplitudes in (a) the eccentricity frequency band of 95–410 ka, (b) the obliquity band of 39–54 ka, (c) the precession band of 19–23 ka, and (d) the semiprecession band 9.5–11.5 ka as predicted by the polynomial model. The units are peak-to-peak differences, assuming a sine waveshape.

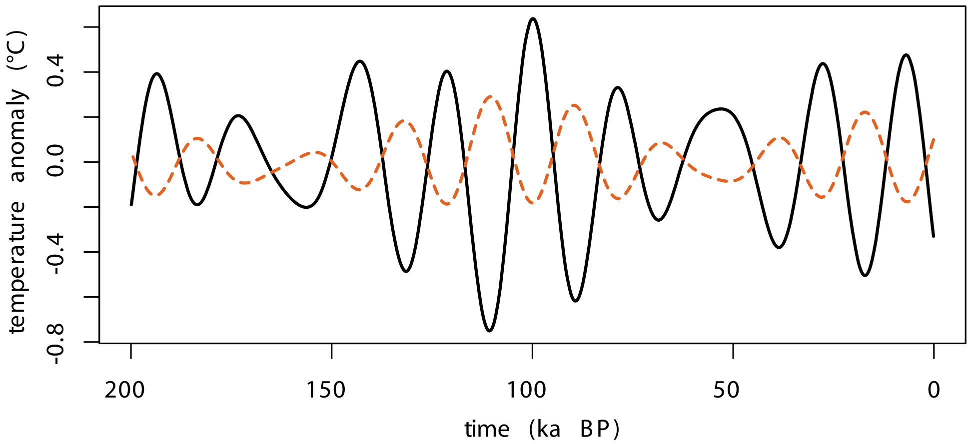

Figure 8. Temperature time series of the last 200 ka as predicted by the polynomial model. North Australia (20°S, 135°E) (black) and Indian Ocean (20°S, 100°E) (red dashed).

insolation minima in the opposite season. The amplitude of the simulated precession signal is a convolution of the amplitude of the forcing, which is strongest in the subtropics, the degree of nonlinearity (generally higher and tropics) and the temperature sensitivity (highest over land).

[42] The shape of the nonlinear response (higher temperature sensitivity in summer or in winter) determines the phase of the precession signal. This is detected in the Holocene analysis where some regions show a cooling trend whereas other regions show a warming trend (Figure 5b). It is also demonstrated by contrasting time series, simulated by the polynomial model, for summer and winter sensitive regions of the same hemisphere. Figure 8 shows a typical example, the temperature time series of North Australia and the Indian Ocean, simulated by the polynomial model. Both show a strong precession signal, but the phases of the precession signal oppose each other although they are forced by the same insolation variability. This phase dependency of the temperature signal on the seasonal sensitivity leads to the intriguing situation that a winter sensitive area in the Southern Hemisphere will perfectly correlate with Northern Hemispheric summer insolation, although driven by local insolation. A similar idea has been proposed for Antarctica by *Stott et al.* [2007], who suggest that sea ice leads to a spring sensitive temperature response and by *Huybers and Denton* [2008] who propose that the nonlinearity of the radiative balance leads to a locally forced precession signal in the Antarctic temperature.

[43] Changes in eccentricity of the Earth's orbit have a small effect on global mean insolation but modulate the amplitude of the precession. A strongly nonlinear temperature response such as in the North Pacific demodulates the eccentricity signal (Figure 7a). In intertropical regions, the Sun comes overhead twice a year at each latitude. In the case of a nonlinear transfer function one of the two insolation maxima gets favored regardless of the time when they occur in the year. As the insolation at spring and autumn equinoxes is out of phase by a half-precession cycle, this leads to the power in the semiprecession band and the eccentricity band (Figures 7a and 7d) [*Ashkenazy and Gildor*, 2008]. This partitioning of the forcing in the intertropical band into eccentricity and semiprecession was also found by *Crowley et al.* [1992] who prescribed a threshold response function to explain the spectra found in Triassic lake deposits. *Berger and Loutre* [1997] and *Berger et al.* [2006] used the maximum insolation during a year as metric to demonstrate that half-precession cycles can be generated from orbital forcing. In contrast to these studies that are based on ad hoc transfer functions, our model shows that the observed present-day transfer function can already explain these frequencies.

[44] Other tools to investigate the problem of the long-term climate response to insolation are Energy Balance Models (EBM). The pioneering work using this technique is that by *Short et al.* [1991] who used a linear, two-dimensional, seasonal EBM to study the spatial pattern of the temperature response to long-term insolation. Their results for the annual mean temperature response [e.g., *Short et al.*, 1991, Figure 9] are similar to our results from the linear model showing only variability in the obliquity band. *Short et al.* [1991] further analyzed the maximum seasonal temperature as diagnostics to obtain a temperature response comparable to the response found in proxy records. In our polynomial template approach, we do not need this assumption and see that the nonlinearities already present in the seasonal cycle lead to a realistic response of the annual mean temperature.

[45] Our concept is related to two recent hypotheses concerning the climate response to insolation variations. The summer energy concept [*Huybers*, 2006; *Huybers and Tziperman*, 2008] provides an explanation for the glacial cycles of the early Pleistocene by proposing that glaciers are sensitive to the integrated summer insolation. This concept is based on the approximation of the annual ablation by positive degree days and the assumption of a linear relationship between temperature and insolation which collaborates with our findings of a linear relationship on extratropical land regions. The integrated summer energy concept and our model address different questions and complement each other. The summer energy model simulates the annual ablation and therefore the response of the glacial mass balance to insolation changes. This question

cannot be addressed by the seasonal template model as changes in the glacial mass balance and their influence on temperature are slow processes not captured in the modern seasonal cycle of temperature. The summer energy concept on the other hand is limited to a specific nonlinear physical mechanism, the ablation. It is therefore not able to resolve other climate feedbacks like the mixed layer depth or monsoon regimes that play an important role in shaping the regional temperature response to insolation.

[46] Recently *Huybers and Denton* [2008] addressed the question of the temperature variability on orbital timescales in Antarctica, proposing that the Antarctic temperature is determined by the local summer duration and not by the summer insolation intensity. The basis for this hypothesis is that the radiative balance indicates greater temperature sensitivity at lower temperatures. This directly relates to the work presented in this paper as a lower sensitivity on warmer temperatures should be detectable in the modern seasonal cycle of temperature. In Antarctica, our analysis suggests a linear or summer sensitive temperature response (section 3.1 and Figure 3) and does therefore not support the summer length hypothesis. More work is needed to understand the reasons and the significance of the discrepancies between the empirical transfer function of insolation and temperature (this study) and the summer length hypothesis [*Huybers and Denton*, 2008]. Potential candidates for the differences include problems with the NCEP reanalysis in Antarctica [*Hines et al.*, 1999] that may lead to artificial summer sensitivity in our study as well as influences on seasonal energy balance in Antarctica, not considered in the summer length hypothesis, which mask or even invert the higher sensitivity to low temperatures given by the radiative balance.

4.3. Limitations of the Concept

[47] The two basic assumptions of our model (time independence and locality) lead to certain limitations. The climate response is time-dependent, and therefore not all feedback processes are captured in our data source, the seasonal cycle. Slow processes like the evolution of ice sheets or changes in the ocean circulation will therefore add more nonlinearities to the system than included by our seasonal template. Furthermore, the boundary conditions which determine the seasonal climate response, and therefore our template, are changing with time. One example is the variation in the sea ice covered area that modifies the position and extent of the winter sensitive regime. This leads to misfits between our data-based model and GCM results in the polar latitudes (Figures 5b and 5c).

[48] The climate system is characterized by pronounced spatial correlations (teleconnections) caused by atmospheric [e.g., *Rimbu et al.*, 2003; *Rodgers et al.*, 2003; *Wallace and Gutzler*, 1981] and ocean dynamics. As the insolation forcing is similar over wide areas, some nonlocal effects are captured by our local approach, but large-scale teleconnections as the NAO cause a misfit of our data-based model in some regions (e.g., Figures 5b and 5c, North Atlantic Region). On long time scales, the large-scale ocean circulation [*Stocker*, 1998] as well as greenhouse gases lead to interhemispheric coupling.

[49] For the comparison of our model predictions with proxy records, one further has to consider that our results are the predicted frequency spectra of the physical quantity temperature. In paleorecords, one might expect altered spectra caused by the additional nonlinearity added by the recorder system [*Crowley et al.*, 1992; *Huybers and Wunsch*, 2003].

5. Conclusions

[50] We propose a simple model for insolation-driven climate variability on astronomical timescales. Under the assumption that the climate response to insolation is the same on seasonal as well as on astronomical timescales we use the observed seasonal cycle of temperature to derive the spatially resolved surface temperature variability of the last 750 ka. Our results show that nonlinearities and feedbacks represented in the observed present-day seasonal cycle have large effects on the long-term climate variability. As one example for the interglacial climate evolution we study the Holocene temperature trends by comparing a linear template model, a nonlinear template model, and a simulation of a complex AOGCM. This model hierarchy allows us to distinguish between linear effects, feedbacks that happen on a seasonal time scale, and long-term feedbacks. The template model therefore acts as a tool for the interpretation of complex model simulations.

[51] Our results have the following implications for the interpretation of paleorecords.

[52] 1. Even at one latitude, different frequency spectra of the temperature evolution are expected, e.g., variability in the obliquity band can dominate in one region whereas variability in the precession band can dominate in another region.

[53] 2. The phase of the astronomically induced temperature changes can vary, depending on the nonlinearity. Regions with a seasonal cycle sensitive to winter insolation (e.g., North Australia) will show a precession signal with a phase opposite to that of summer sensitive areas (Figure 8). This leads to the intriguing situation that a winter sensitive area in the Southern Hemisphere will perfectly correlate with Northern Hemispheric summer insolation, even if it is driven by local insolation.

[54] 3. In tropical areas, a temperature signal in the eccentricity band as well as in the semiprecession band is predicted with significant amplitude. This corresponds well with results from *Crowley et al.* [1992], *Berger and Loutre* [1997], and *Berger et al.* [2006] with the difference that we did not have to prescribe a specific transfer function. The simultaneous appearance of semiprecession and eccentricity which is found in paleodata [*Rutherford and D'Hondt*, 2000] can be directly explained by a nonlinear response to the local insolation.

[55] 4. The land-sea pattern modulates the amplitude of the temperature response. This corresponds well with the results found by *Short et al.* [1991], who used an EBM to study the temperature response on orbital forcing. For the annual mean temperatures, we observe two competing effects: The larger heat capacity of the ocean damps the temperature response, but the generally higher nonlinearity

over the ocean amplifies the response on the precession forcing. The obliquity response is generally stronger over land, but the precession response does not show a clear ocean/land classification.

[56] On the basis of the comparison to a Holocene GCM experiment [*Lorenz et al.*, 2006; *Lorenz and Lohmann*, 2004], we propose our result as lower estimate of the regional effects of insolation. Large-scale changes like the buildup and retreat of ice sheets and their effect on the global mean temperature add up to these effects. In this way, our model can be seen as a complementary concept to the common approach of relating climate records from all over the world to 65°N summer insolation. It remains open whether the local effects we found may influence the global scale. The tropical temperature variability that we found in the eccentricity and semiprecession band might act on the high-latitude climate via teleconnections [e.g., *Cane*, 1998; *Huybers and Molnar*, 2007; *Rodgers et al.*, 2003]. This interplay of local and global effects remains open for further studies.

[57] Our results are also a reminder to be careful in using orbital tuning to date paleorecords. The amplitudes that our model predicts for the temperature response on local insolation have a magnitude similar to that of reconstructed glacial-interglacial changes in tropical and subtropical latitudes [*Farrera et al.*, 1999; *Pflaumann et al.*, 2003]. This implies that the surface temperatures and related climate variables are not globally correlative, and even spatially close records may differ in their phasing. Therefore, using some ad hoc tuning target as the 65°N summer insolation to determine the time scale of proxy records might not be justified.

[58] The method of using the seasonal cycle as template can also be applied for other variables, such as precipitation or dust. Here a locally measured seasonal cycle can be used to predict the local response to orbital insolation changes and give a starting point for the interpretation of paleorecords.

[59] **Acknowledgments.** This study was funded by the Helmholtz Association through the programs MARCOPOLI and PACES. We would like to thank Andrea Bleyer for her help in preparing this manuscript. This paper benefited from discussions with Frank Lamy and Klaus Grosfeld. We are grateful to the reviewers Lorraine E. Lisiecki and Peter Huybers, as well as to Gerald Dickens, for their detailed comments on the manuscript.

References

Adhémar, J. (1842), *Révolutions de la Mer*, Carilian-Goeury et V. Dalmont, Paris.

Ashkenazy, Y., and H. Gildor (2008), Timing and significance of maximum and minimum equatorial insolation, *Paleoceanography*, *23*, PA1206, doi:10.1029/2007PA001436.

Berger, A. L. (1978), Long-term variations of daily insolation and quaternary climatic changes, *J. Atmos. Sci.*, *35*(12), 2362–2367, doi:10.1175/1520-0469(1978)035<2362:LTVODI>2.0.CO;2.

Berger, A., and M. Loutre (1991), Insolation values for the climate of the last 10 million years, *Quat. Sci. Rev.*, *10*(4), 297–317, doi:10.1016/0277-3791(91)90033-Q.

Berger, A., and M. F. Loutre (1997), Intertropical latitudes and precessional and half-precessional cycles, *Science*, *278*(5342), 1476–1478, doi:10.1126/science.278.5342.1476.

Berger, A., M. F. Loutre, and J. L. Mélice (2006), Equatorial insolation: From precession harmonics to eccentricity frequencies, *Clim. Past*, *2*(2), 131–136.

Biasutti, M., D. S. Battisti, and E. S. Sarachik (2003), The annual cycle over the tropical Atlantic, South America, and Africa, *J. Clim.*, *16*(15), 2491–2508, doi:10.1175/1520-0442(2003)016<2491:TACOTT>2.0.CO;2.

Bloomfield, P. (1976), *Fourier Analysis of Time Series: An Introduction*, John Wiley, New York.

Broecker, W. S., and J. van Donk (1970), Insolation changes, ice volumes, and the O^{18} record in deep-sea cores, *Rev. Geophys.*, *8*, 169–198, doi:10.1029/RG008i001p00169.

Cane, M. A. (1998), Climate change: A role for the tropical Pacific, *Science*, *282*(5386), 59–61, doi:10.1126/science.282.5386.59.

Carton, J. A., and Z. Zhou (1997), Annual cycle of sea surface temperature in the tropical Atlantic Ocean, *J. Geophys. Res.*, *102*(C13), 27,813–27,824, doi:10.1029/97JC02197.

Clemens, S., W. Prell, D. Murray, G. Shimmield, and G. Weedon (1991), Forcing mechanisms of the Indian Ocean monsoon, *Nature*, *353*(6346), 720–725, doi:10.1038/353720a0.

Clement, A. C., A. Hall, and A. J. Broccoli (2004), The importance of precessional signals in the tropical climate, *Clim. Dyn.*, *22*(4), 327–341, doi:10.1007/s00382-003-0375-8.

Croll, J. (1875), *Climate and Time in Their Geological Relations: A Theory of Secular Changes of the Earth's Climate*, Daldy Tsbister, London.

Crowley, T. J., K. Y. Kim, J. G. Mengel, and D. A. Short (1992), Modeling 100,000-year climate fluctuations in pre-Pleistocene time-series, *Science*, *255*(5045), 705–707, doi:10.1126/science.255.5045.705.

Farrera, I., et al. (1999), Tropical climates at the Last Glacial Maximum: A new synthesis of terrestrial palaeoclimate data. I. Vegetation, lake-levels and geochemistry, *Clim. Dyn.*, *15*(11), 823–856, doi:10.1007/s003820050317.

Ganopolski, A., C. Kubatzki, M. Claussen, V. Brovkin, and V. Petoukhov (1998), The influence of vegetation-atmosphere-ocean interaction on climate during the mid-Holocene, *Science*, *280*(5371), 1916–1919, doi:10.1126/science.280.5371.1916.

Hays, J. D., J. Imbrie, and N. J. Shackleton (1976), Variations in the Earth's orbit: Pacemaker of the ice ages, *Science*, *194*(4270), 1121–1132, doi:10.1126/science.194.4270.1121.

Held, I. (2005), The gap between simulation and understanding in climate modeling, *Bull. Am. Meteorol. Soc.*, *86*(11), 1609–1614, doi:10.1175/BAMS-86-11-1609.

Hines, K. M., R. W. Grumbine, D. H. Bromwich, and R. I. Cullather (1999), Surface energy balance of the NCEP MRF and NCEP-NCAR reanalysis in Antarctic latitudes during FROST, *Weather Forecasting*, *14*(6), 851–866, doi:10.1175/1520-0434(1999)014<0851:SEBOTN>2.0.CO;2.

Huybers, P. (2006), Early Pleistocene glacial cycles and the integrated summer insolation forcing, *Science*, *313*(5786), 508–511, doi:10.1126/science.1125249.

Huybers, P., and G. Denton (2008), Antarctic temperature at orbital timescales controlled by local summer duration, *Nat. Geosci.*, *1*(11), 787–792, doi:10.1038/ngeo311.

Huybers, P., and P. Molnar (2007), Tropical cooling and the onset of North American glaciation, *Clim. Past*, *3*(3), 549–557.

Huybers, P., and E. Tziperman (2008), Integrated summer insolation forcing and 40,000-year glacial cycles: The perspective from an ice-sheet/energy-balance model, *Paleoceanography*, *23*, PA1208, doi:10.1029/2007PA001463.

Huybers, P., and C. Wunsch (2003), Rectification and precession signals in the climate system, *Geophys. Res. Lett.*, *30*(19), 2011, doi:10.1029/2003GL017875.

Imbrie, J., et al. (1992), On the structure and origin of major glaciation cycles: 1. Linear responses to Milankovitch forcing, *Paleoceanography*, *7*, 701–738, doi:10.1029/92PA02253.

Jackson, C. S., and A. J. Broccoli (2003), Orbital forcing of Arctic climate: Mechanisms of climate response and implications for continental glaciation, *Clim. Dyn.*, *21*(7–8), 539–557, doi:10.1007/s00382-003-0351-3.

Kalnay, E., et al. (1996), The NCEP/NCAR 40-year reanalysis project, *Bull. Am. Meteorol. Soc.*, *77*(3), 437–471, doi:10.1175/1520-0477(1996)077<0437:TNYRP>2.0.CO;2.

Kara, A. B., P. A. Rochford, and H. E. Hurlburt (2003), Mixed layer depth variability over the global ocean, *J. Geophys. Res.*, *108*(C3), 3079, doi:10.1029/2000JC000736.

Laskar, J., P. Robutel, F. Joutel, M. Gastineau, A. C. M. Correia, and B. Levrard (2004), A long-term numerical solution for the insolation quantities of the Earth, *Astron. Astrophys.*, *428*(1), 261–285, doi:10.1051/0004-6361:20041335.

Lau, W. K. M., K. M. Kim, and M. I. Lee (2007), Characteristics of diurnal and seasonal cycles in global monsoon systems, *J. Meteorol. Soc. Jpn.*, *85A*, 403–416, doi:10.2151/jmsj.85A.403.

Liu, Z., S. P. Harrison, J. Kutzbach, and B. Otto-Bliesner (2004), Global monsoons in the mid-Holocene and oceanic feedback, *Clim. Dyn.*, *22*(2–3), 157–182.

Lohmann, G., S. J. Lorenz, and M. Prange (2005), Northern high-latitude climate changes during the Holocene as simulated by circulation models, in *The Nordic Seas: An Integrated Perspective—Oceanography, Climatology, Biogeochemistry, and Modeling*, *Geophys. Monogr. Ser.*, vol. 158, edited by H. Drange et al., pp. 273–288, AGU, Washington, D. C.

Lorenz, S. J., and G. Lohmann (2004), Acceleration technique for Milankovitch type forcing in a coupled atmosphere-ocean circulation model: Method and application for the Holocene, *Clim. Dyn.*, *23*(7–8), 727–743, doi:10.1007/s00382-004-0469-y.

Lorenz, S. J., J.-H. Kim, N. Rimbu, R. R. Schneider, and G. Lohmann (2006), Orbitally driven insolation forcing on Holocene climate trends: Evidence from alkenone data and climate modeling, *Paleoceanography*, *21*, PA1002, doi:10.1029/2005PA001152.

Loutre, M. F., D. Paillard, F. Vimeux, and E. Cortijo (2004), Does mean annual insolation have the potential to change the climate?, *Earth Planet. Sci. Lett.*, *221*(1–4), 1–14, doi:10.1016/S0012-821X(04)00108-6.

Milankovitch, M. (1941), *Kanon der Erdbestrahlung und Seine Anwendung auf das Eiszeitenproblem*, vol. 133, 633 pp., Akad. R. Serbia, Belgrade.

Pahnke, K., and J. P. Sachs (2006), Sea surface temperatures of southern midlatitudes 0–160 kyr B.P., *Paleoceanography*, *21*, PA2003, doi:10.1029/2005PA001191.

Pahnke, K., R. Zahn, H. Elderfield, and M. Schulz (2003), 340,000-year centennial-scale marine record of Southern Hemisphere climatic oscillation, *Science*, *301*(5635), 948–952.

Pflaumann, U., et al. (2003), Glacial North Atlantic: Sea-surface conditions reconstructed by GLAMAP 2000, *Paleoceanography*, *18*(3), 1065, doi:10.1029/2002PA000774.

Rayner, N. A., D. E. Parker, E. B. Horton, C. K. Folland, L. V. Alexander, D. P. Rowell, E. C. Kent, and A. Kaplan (2003), Global analyses of sea surface temperature, sea ice, and night marine air temperature since the late nineteenth century, *J. Geophys. Res.*, *108*(D14), 4407, doi:10.1029/2002JD002670.

Rimbu, N., G. Lohmann, J.-H. Kim, H. W. Arz, and R. Schneider (2003), Arctic/North Atlantic Oscillation signature in Holocene sea surface temperature trends as obtained from alkenone data, *Geophys. Res. Lett.*, *30*(6), 1280, doi:10.1029/2002GL016570.

Rodgers, K. B., G. Lohmann, S. Lorenz, R. Schneider, and G. M. Henderson (2003), A tropical mechanism for Northern Hemisphere deglaciation, *Geochem. Geophys. Geosyst.*, *4*(5), 1046, doi:10.1029/2003GC000508.

Rubincam, D. P. (1994), Insolation in terms of Earth's orbital parameters, *Theor. Appl. Climatol.*, *48*(4), 195–202, doi:10.1007/BF00867049.

Rutherford, S., and S. D'Hondt (2000), Early onset and tropical forcing of 100,000-year Pleistocene glacial cycles, *Nature*, *408*(6808), 72–75, doi:10.1038/35040533.

Short, D. A., J. G. Mengel, T. J. Crowley, W. T. Hyde, and G. R. North (1991), Filtering of Milankovitch cycles by Earth's geography, *Quat. Res.*, *35*(2), 157–173, doi:10.1016/0033-5894(91)90064-C.

Stocker, T. F. (1998), Climate change: The seesaw effect, *Science*, *282*(5386), 61–62, doi:10.1126/science.282.5386.61.

Stott, L., A. Timmermann, and R. Thunell (2007), Southern Hemisphere and deep-sea warming led deglacial atmospheric CO_2 rise and tropical warming, *Science*, *318*(5849), 435–438, doi:10.1126/science.1143791.

Tuenter, E., S. L. Weber, F. J. Hilgen, and L. J. Lourens (2003), The response of the African summer monsoon to remote and local forcing due to precession and obliquity, *Global Planet. Change*, *36*(4), 219–235, doi:10.1016/S0921-8181(02)00196-0.

Wallace, J. M., and D. S. Gutzler (1981), Teleconnections in the geopotential height field during the Northern Hemisphere winter, *Mon. Weather Rev.*, *109*(4), 784–812, doi:10.1175/1520-0493(1981)109<0784:TITGHF>2.0.CO;2.

Wohlfahrt, J., S. P. Harrison, and P. Braconnot (2004), Synergistic feedbacks between ocean and vegetation on mid- and high-latitude climates during the mid-Holocene, *Clim. Dyn.*, *22*(2–3), 223–238, doi:10.1007/s00382-003-0379-4.

T. Laepple and G. Lohmann, Alfred Wegener Institute for Polar and Marine Research, Bussestrasse 24, D-27570 Bremerhaven, Germany. (thomas.laepple@awi.de)